TDK THESIS

Tudományos Diákköri Konferenciáján

Floriane LOUBOUTIN

2022

The University of Veterinary Medicine

Department of Ecology

Neuronal sorting nexins and Seizure-related gene 6 trafficking and their influence in the dendritic integration

Floriane LOUBOUTIN

Supervisor: Eszter BEREKMÉRI (Research fellow)

Budapest 2022

Table of content

1 List of abbreviations

AD	Alzheimer's disease
AP	Action potential
APP	Amyloid Precursor Protein
BACE1	Beta-site APP-Cleaving Enzyme 1
E15	Embryonic day 15
EE	Early endosome
EEA1	Early Endosomal Antigen 1
EPSP	Excitatory postsynaptic potentials
DIV	Days in vitro
KO	Knock-out
LE	Late endosome
NMDA	N-methyl-D-aspartate
PSD-95	Postsynaptic density protein 95
PTZ	Pentylenetetrazole
PX	Phox-homology
RE	Recycling endosome
ROI	Region of interest
Sez-6	Seizure-related gene-6
Sez-6 -/-	Sez-6 KO
Sez-6 KO - PSD	Post synaptic density site is included in Sez-6 KO model
SNX	Sorting nexins
TfR-mCh	Transferrin receptor-mCherry
WT	Wild type

2 INTRODUCTION

The development of appropriate neuronal circuitry in the mammalian central nervous system is a complex process, essential for learning, memory and cognition. Indeed, the development of neurons requires precisely controlled systems that ensure the formation of proper cellular morphology and the connections between neurons.

2.1 Seizure-related gene 6 (Sez-6)

Sez-6 plays an important role in this process being a brain-specific protein that has been found to be crucial for the development of dendrites and excitatory synapses. Knock-out (KO) of the Sez-6 gene in mice (causing loss of all Sez-6 protein isoforms) results in an immature morphology in cultured cortical pyramidal neurons (14 days in vitro, DIV). These neurons present a greater number of short dendritic branches (Figure 1) and lower excitatory synapse density (Figure 2) with a corresponding decrease in neuronal excitability compared to wild-type (WT) neurons (Gunnersen et al., 2007).
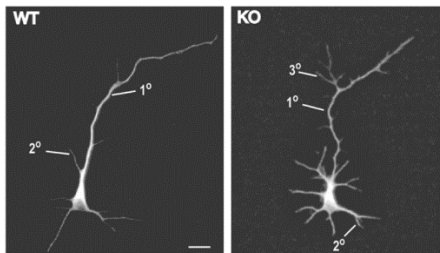
Figure 1 : Primary cultured cortical neurons from Sez-6 null mutant mice embryos display increased numbers of short neurites. Figure from Gunnersen et al., 2007.

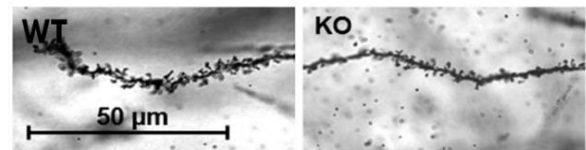*Figure 2 :* Sez-6 KO neurons show reduced spine density on dendrites, which correlates with a reduction in PSD-95 levels. Figure from Gunnersen et al., 2007.

A likely involvement of Sez-6 in dendritic development and synaptogenesis is indicated by its spatiotemporal expression pattern in the mouse brain. Cortical expression of Sez-6 changes with developmental stage: Sez-6 protein levels were high at embryonic day 15 (E15) in the developing neocortex and decrease after birth (Kim et al., 2002); (Gunnersen et al., 2007); (Osaki et al., 2011). Indeed, achievement of dendrite elongation and branching during the establishment of a complex dendritic arbor and the development of appropriate excitatory synaptic connectivity are two processes that are thought to be intrinsically linked in early development.

2.1.1   Sez-6 and neural computation

As dendrites are the sites of most synapses on neuron, proper growth and arborization of dendrites are clearly crucial for nervous system function. Consequently, the results of defects in dendrite growth are profound, often accompanying severe neurodevelopmental disorders, because the propagation of action potential (AP) in dendrites depends on dendritic morphology (Vetter et al., 2001). And in the case of Sez-6, neurons lacking Sez-6 show reduced excitatory postsynaptic potentials (EPSPs) (Gunnersen et al., 2007) (Figure 3).
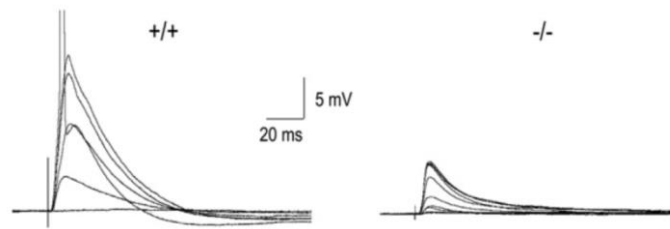
Figure 3 : Summating EPSPs recorded in pyramidal neurons. The EPSP increased in amplitude, reached threshold and evoked an AP in WT (+/+) mice. In Sez-6 null (-/-) mice, synaptic stimulation led to much smaller summation, and the EPSP did not reach threshold. Figure from Gunnersen et al., 2007.

Altogether, shorter and increased dendritic branching of neurons in the KO cortex as well as reduced EPSP suggest possible functional differences in synaptic connections, compared with WT cortex. In this manner, we could imagine that WT and KO neurons present specific models of dendritic trees that determine the nature and number of synapses that a neuron receives. In this way their dendrite skeletons could have highly specified membrane properties that define the computational ability of each neuron (McAllister, 2000). Actually, neural computation relies on the integration of synaptic inputs across a neuron's dendritic arbor (Ran et al., 2020).

Modeling single-neuron dynamics is the first step to quantitatively understand brain computation (Li et al., 2019). Thus, in this report, neuron modelling could help us to identify the importance of Sez-6 in the creation of the appropriate dendritic morphology in order to trigger AP necessary for the proper functioning of the brain. In this way passive cable and compartmental models need to be set in relation to the classical cable theory. This latter principle constructs biologically realistic membranes, and neurites are modeled as cylinders composed of segments with capacitances and resistances according to Hodgkin–Huxley model. Virtual connectivity and electrophysiology tools are combined to drive and measure AP generation and propagation in neural network.

2.1.2   Sez-6 and endocytosis

Functional neural networks are shaped by synapse formation (Ahmari & Smith, 2002). And conversely, a complex regulatory circuit influences excitatory synaptogenesis, which has been shown to be in part regulated by Sez-6 (Gunnersen et al., 2007).

Interestingly, Sez-6 was first identified in a study that sought to discover new genes involved in epilepsy (Shimizu-Nishikawa, Kajiwara, & Sugaya, 1995). Mouse cortical neurons treated with pentylenetetrazole (PTZ), a convulsant drug, exhibited increased expression of Sez-6 mRNA. This PTZ-upregulated gene encodes three protein isoforms resulting from alternate mRNA splicing (Figure 4). Type I and type II isoforms of Sez-6 are transmembrane cell-surface proteins with long N-terminal extracellular domains and short C-terminal cytoplasmic domains. The Sez-6 type III isoform arises from an alternatively spliced mRNA transcript that produce a truncated secreted form of the protein, differing from type I and type II by a short sequence of hydrophobic amino acids at the C-terminal. Furthermore Sez-6tII has recently been found to be cleaved by β-secretase or BACE1 (Beta-site APP-Cleaving Enzyme 1) (Kuhn et al., 2012). This enzyme plays a critical role in the processing of Amyloid Precursor Protein (APP) to generate the amyloidogenic Aβ peptide - the neurotoxic peptide responsible for neurodegeneration in Alzheimer's disease (AD) - and is implicated in the development and progression of AD. All three Sez-6 isoforms contain Threonine-rich regions and the known protein-protein interaction domains, SCR (Short Consensus Repeat) and CUB (Complement subcomponent (C1r, C1s) / sea Urchin embryonic growth factor (Uegf) / Bone morphogenetic protein 1) (Shimizu-Nishikawa, Kajiwara, Kimura, et al., 1995) which have been linked to the regulation of dendrite and synapse formation in other proteins (Gally et al., 2004).
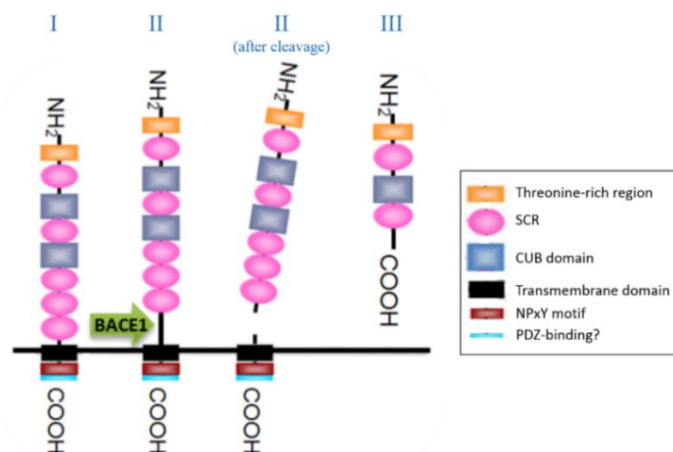

Figure 4 : Sez-6 protein isoforms structure. Figure adapted from Shimizu-Nishikawa et al., 1995b

The presence of SCR and CUB domains, generally involved in cell adhesion and recognition, implies that Sez-6 protein activity involve binding to other extracellular or cell-surface proteins.

The Sez-6 tII, being a transmembrane cell-surface protein can undergo endocytosis (Figure 5). After internalization in early endosome (EE), transmembrane proteins can be recycled back to the cell surface via recycling endosome (RE), enter late endosomal (LE) and lysosomal compartments for degradation or transported retrogradely to the trans-Golgi network (Rink et al., 2005). A precise regulation of these pathways has been shown to be really important in such diverse processes as cytokinesis, cell adhesion, cell fusion, learning and memory (Grant & Donaldson, 2009). However, whether the trafficking and cell-surface distribution of Sez-6 is regulated, and how transmembrane Sez-6 is distributed amongst these various compartments, is not known.
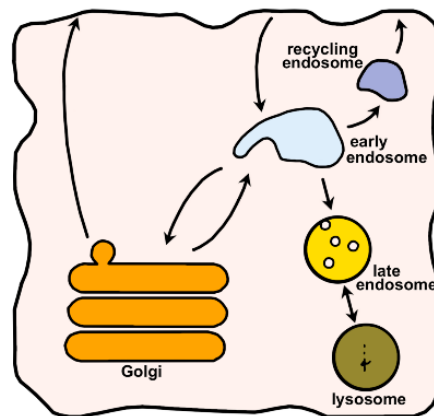
Figure 5 : The endosomal-lysosomal pathway. Figure adapted from Adapted from Teasdale, Collins, 2012.

2.2   Neuronal sorting nexins (SNXs)

Protein sorting into subcellular or recycling compartments is emerging as an important mechanism for regulating protein function. In the case of Sez-6, the sorting nexins SNX17 and SNX27 could be involved in these processes. An interesting property of these SNXs is that they are highly expressed in neurons, and therefore they will be referred as neuronal SNXs in this report.

The Phox-homology (PX) domain proteins (Figure 6), most of which are classified as SNXs, constitute an extremely diverse family of molecules that play varied roles in cell trafficking, cell signaling, membrane remodeling and organelle motility (Teasdale & Collins, 2012). They are essential for endosomal cargo interactions, endosomal scaffolding and

trafficking functions via their C-terminal FERM domain (4.1 protein / Ezrin / Radixin / Moesin). FERM domain has all three modules of a typical FERM domain (F1, F2 and F3). It binds target molecules through their cytoplasmic NPxY motifs (Asn-Pro-Xaa-Tyr) and this motif is present in the transmembrane forms of Sez-6 (Figure 4). The N-terminal PX domain of these proteins regulate endosomal localization by Ptd-Ins-3-P binding (Phosphatidyl-Inositol-3-Phosphates), marker of organelle identity in the endocytic system. Additionally, SNX27 has an N-terminal PDZ domain (Postsynaptic density 95 / Discs large / Zonula occludens), which could interact with the putative PDZ binding region of Sez-6 (Figure 4).
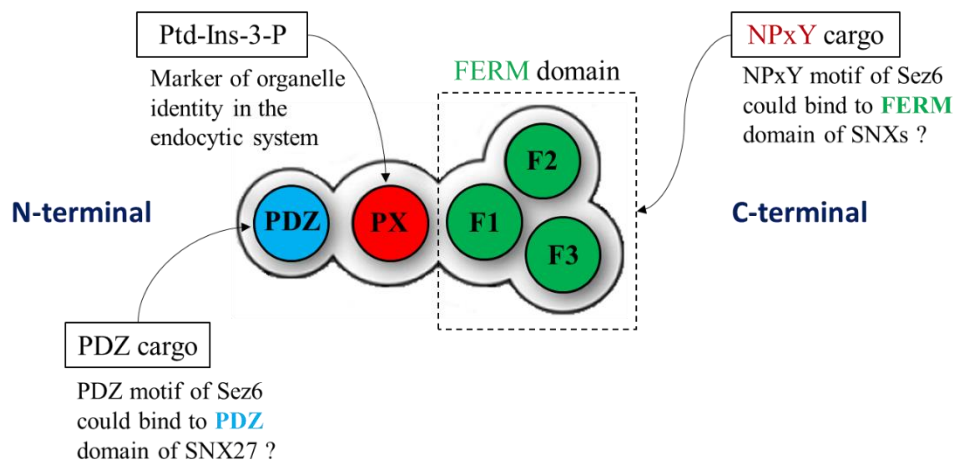
Figure 6 : Molecular interactions regulated by the PX-FERM proteins in endosomal membrane transport and signaling. They contain a C-terminal FERM domain (binds to NPxY), a N-terminal PX domain (binds to PtdIns3P) and, in the case of SNX27, an N-terminal PDZ domain (binds to PDZ cargo). Figure adapted from Teasdale, Collins, 2012

SNX17 is implicated directly in the recycling of APP from endosomes to the cell surface, as it binds to the APP NPxY sorting motif. This activity results in an increased level of APP breakdown and amyloid Aβ peptide production within the endosomal compartment. (Teasdale & Collins, 2012). As SNX17 serves as an intracellular adaptor protein for APP and regulates its trafficking and processing to Aβ (Lee et al., 2008), it could be involved in Sez-6 trafficking. The role of SNX27 in trafficking its target molecules from endosomes to cell membrane has been shown for the NMDA receptor 2C (Cai et al., 2011). Thus, these two distinct PX-FERM proteins which are key regulators of recycling from endosomes to the cell surface via binding PDZ and/or NPxY recycling signals, could be important for the trafficking of Sez-6.

2.3 Rab GTPase proteins

The Rab small GTPases are crucial elements of the machinery that controls membrane traffic apparatus, and each step involves a different Rab protein (Figure 7). Endosomes are characterized by specific combinations of these Rab proteins which intercommunicate (Sönnichsen et al., 2000) and which undergo a conversion mechanism between each compartment (Rink et al., 2005). Over 60 Rab proteins in mammals have distinct localizations and of the Rab proteins associated with regulation of endosomal traffic, Rab5 and Rab11 have been studied the most, as two regulatory components of the transport machinery (Grant & Donaldson, 2009). Rab5 has been defined as a small GTPase protein associated with the plasma membrane and EE. On the other hand, the RE compartment has been itself defined by the presence of Rab11 which is required for its functions. On the other side Rab7 and Rab9 are recruited onto LE.
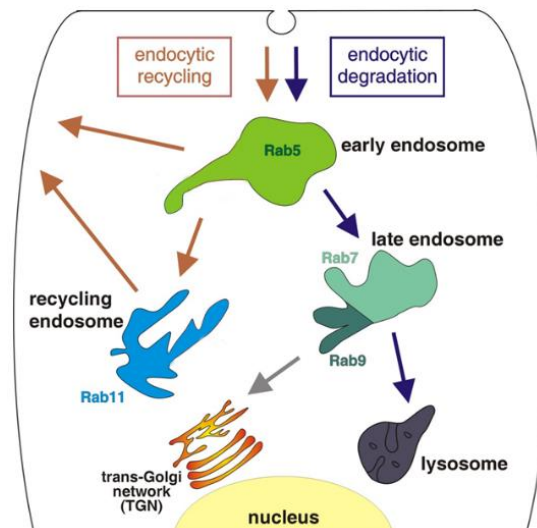
Figure 7 : The domain distribution of Rab proteins describing endocytic organelles. Figure adapted from Sönnichsen et al., 2000.

3   Aims

This study was firstly conducted to investigate the hypothesis that Sez-6 is of a great importance in signal propagation depending on neuron morphology. To this aim, we built a model of computational simulation of the dendritic integration processes. We then compared the efficacy of WT neurons and Sez-6 -/- neurons to integrate a stimulus in the spatiotemporal neural network.

My second aim is to highlight that Sez-6 is trafficked by SNX17 and SNX27. To provide evidence in support of this hypothesis, I will firstly determine the subcellular locations of Sez-6, SNX17 and SNX27 using markers of endosomal compartments. Our preliminary data has shown that SNX17 and SNX27 are not localized in the LE compartments marked by Rab7 and Rab9. For this reason, I focused my study on the EE and RE, marked by Rab5/SNX1 and Rab11, respectively.

Finally, my third aim is to determine whether there is a biochemical interaction between Sez-6 and either of the neuronal SNXs. For these experiments, recombinant proteins produced in COS-cells were co-immunoprecipitated and analyzed by Western blot. Different combinations of tagged Sez-6, SNX17 and SNX27 constructs were used to determine whether Sez-6 and neuronal SNXs physically interact or participate in shared protein complexes.

4 MATERIALS & METHODS

4.1 Computational simulation of the dendritic integration processes

4.1.1 Generating morphometric data

Firstly, to investigate the Sez-6 molecule expression effect on the dendritic integration processes in cortical pyramidal cells in mice, previously published morphometric data was asked and collected from Jenny Gunnersen's laboratory (University of Melbourne, Department of Anatomy and Physiology; (Gunnersen et al., 2007).

Sez-6 homozygous null controls were produced by intercross of Sez-6 heterozygote mice (129/SvJ x C57BL/6J background). E15.5 mouse embryos were obtained for the culture of primary cortical neurons in WT and Sez-6 -/- lines. The cells were spread on coverslips and then fixed and dyed with rabbit anti-PSD-95 primary antibody (postsynaptic density protein 95) against the C-terminal region of human PSD-95 (Zymed Labs., San Francisco, CA; 1/200). Alexa Fluor 594 conjugated anti-rabbit IgG (H+L) has been used as a secondary antibody. Confocal images were made using a Zeiss LSM5 Pascal microscope. 20 neurons per coverslip had been acquired with a 63x oil lens. Eight-bit Z-stack digital images of the fluorescence emission at 594 nm were converted into merged maximum intensity projection images using Zen 2009 software (Zeiss, Germany). Files were saved in tiff format. Eight WT neurons and eight Sez-6 -/- neurons were collected and segmented by the plug-in Neurotracer in FIJI (version ImageJ 2.0.0-rc-65/1.52n) and saved in swc file format. During the segmentation we also used the filled option to save the diameters of the dendritic branches.

4.1.2 Simulating the inputs

During the simulation, Python 3 was used in Colab notebook environment with packages NEURON (for adding the equations of the neuronal simulations), Matplotlib (for plotting the results), NumPy (for mathematical calculations), Random (for choose random locations during the simulations) and Pandas (for spreadsheet management).

For the simulations we add passive mechanism to each dendritic branches and divided all branches to 1 µm long sections. Firstly, we hypothesized that all these sections are capable to get a synaptic input. An input was strictly defined by the NEURON package ExpSyn

function: only 1 input arrived to the randomly chosen dendritic section, not weighted. The equation behind the synaptic current (i) change was:

$$i = weight \cdot e^{\frac{-t}{\tau}} \cdot V_m$$

Dendrites were modelled as cables according to the cable theory: dendrites could be simplified to passive cylinders where the input signals decay over space and time (which involves partial differential equations mathematically). With a space constant (λ) and a time constant (τ), the signal spatiotemporal decay is easier to follow and could be expressed with an equation:

$$\frac{\partial V}{\partial T} = -V + \frac{\partial^2 V}{\partial X^2}$$

Where the voltage (V) is equivalent to the difference of the membrane potential (Vm) and the resting membrane potential (Vr): $V = V_m - V_r$

The X and T contain the spatial and temporal, respectively, properties of the cell membrane: $X = \frac{x}{\lambda}$ and $T = \frac{t}{\tau}$

Where the spatial constant (λ) is the square root of the ratio of the membrane resistance (r_m) over the intracellular resistance (r_i) per unit length of the cable. This is the same as the square root of the ratio of the unit membrane area resistance (R_m) over the resistance of the intracellular medium (R_i) multiplied by the quarter of the diameter of the cable (d):

$$\lambda = \sqrt{(r_m/r_i)} = \sqrt{\{(R_m/R_i) \cdot (d/4)\}}$$

The time constant calculated from the membrane resistance (r_m) and the membrane capacitance (c_m) (capital letters represents the calculations per unit):

$$\tau = r_m c_m = R_m C_m$$

The main parameters in the simulation were:

$R_{m_{dendritic}} = 13\ M\Omega$ $\qquad$ $R_{m_{somatic}} = 100\ M\Omega$ $\qquad$ $V_r = -65\ mV$ $\qquad$ $C_m = 1\ \frac{\mu F}{cm^2}$

To see the integration processes, we added different number of inputs (from 1 to 10) in randomly selected dendritic sections (compartmental modeling). All input number was tested 10 times in each neuron (Figure 8).

A) 1 input   **B) 10 inputs**
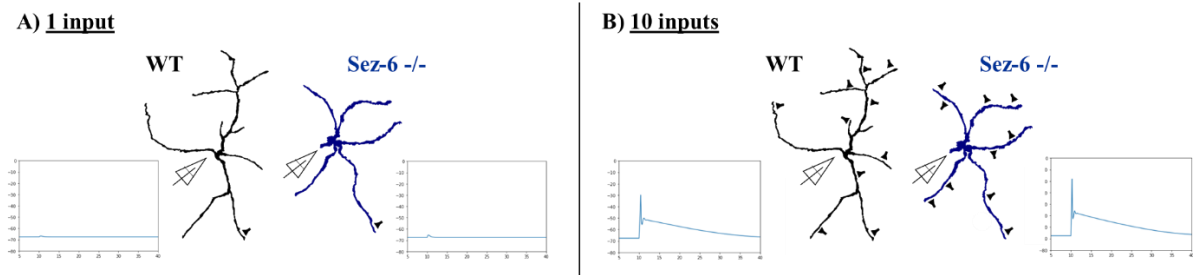
Figure 8 : Simulations to investigate the temporal integration processes of the neurons. During the simulations we randomly located the same input (symbolized by the synaptic terminals on the figure) on the different dendritic branches on WT (black) and Sez-6 -/- (blue) neurons. The number of the inputs started from 1 (A) and went to 10 (B). Each input number were tested by 10 times. The results of the integration processes were measured in the soma (symbolized by a schematic patch clamp electrode). Example voltage curves are presented here (x axis: time in ms and y axis voltage in mV).

The integrated signals were measured in mV in the soma of the neuron. After this simulation, we include the reported decreased post synaptic density in case of Sez-6 -/- mice in our model (Gunnersen et al., 2007). Thus, we repeated the simulations on the Sez-6 -/- neurons, and each input had only a 75% chance of occurring during the simulation (Figure 9).

A) 10 inputs in Sez-6 -/-   **B) 75% of total input in Sez-6 -/-**
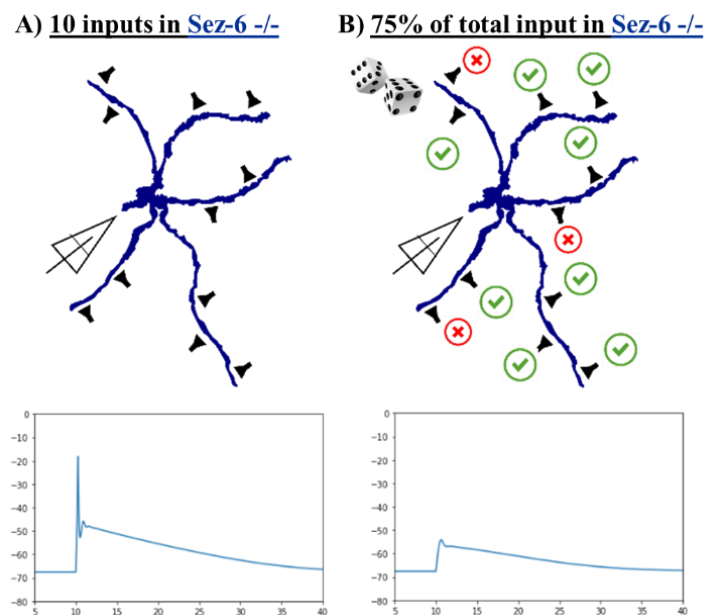
Figure 9 : Simulations to investigate the temporal integration processes of the neurons including the reported loss of synaptic places. In KO animals the number post synaptic density was decreased by 25%. To replicate this result, we decreased all synaptic input existence probability by 25%. Example voltage curves are presented here (x axis: time in ms and y axis voltage in mV).

In this manner we had three different simulated groups depending on their morphology: WT, Sez-6 -/- (Sez-6 KO) and the reported post synaptic density site included in the model of Sez-6 -/- (Sez-6 KO - PSD).

4.1.3 Data analysis

For testing the morphological data, we measured the averages of the dendrite length and diameters. The normal distribution was tested by Shapiro-Wilk test and the differences between WT and Sez-6 -/- were tested with Welch two sampled t-test (in case of the length of the dendrites) and Wilcoxon test (in case of the diameters).

In all simulation turns, the randomly chosen input distances were saved. Linear mixed-effects model was used to analyze how the average distances of the inputs, the number of the inputs and the type of the neuron were affecting the maximal voltage reached (at the soma of the cells). The cell identification number was used as a random effect variable.

4.2 Subcellular localization of Sez-6, SNX17 and SNX27 in endosomal compartments

4.2.1 Primary cortical neuron culture

4.2.1.1 *Glass coverslips preparation*

In the second part of my thesis, 18mm diameter glass coverslips (Menzel-Gläser CS13100, Grayle Scientific, Australia) were used for culturing primary cortical neuron. They were washed for approximately 2 hours in absolute ethanol and at least 1 hour in 70% ethanol. Coverslips were placed under UV light for 25 min, air-dried and coated with 300μL of sterile filtered (0.22μm filter, Millipore, USA) 0.5mg/mL poly-D-lysine hydrobromide (PDL, Sigma, USA) in borate buffer prior to incubation overnight at 4°C. Coverslips were washed 3x5 min in Dulbecco's phosphate buffered saline (DPBS; Gibco). 18mm coverslips were placed in wells of 12 well-plates (Thermo Fisher Scientific, USA), covered with laminin (10μg/mL, Invitrogen) in sterile DPBS, and incubated for at least 4 hours at 37°C, 5% CO_2. Laminin was aspirated off immediately prior to plating cells.

4.2.1.2 *Tissue collection*

Mouse embryos were obtained for the culture of primary neurons from timed matings of C57BL6/J mice. All animal procedures involving animals were approved by the Anatomy & Neuroscience, Pathology, Pharmacology, and Physiology Animal Ethics Committee at the University of Melbourne.

E15.5 mouse embryos were placed on ice for 5 min in order to anaesthetize them by hypothermia prior to decapitation. Brains were dissected out and placed in 3cm Petri dishes (Thermo Fisher Scientific) filled with DPBS. Cortices were dissected away from other brain structures and collected in Eppendorf tubes containing sterile DPBS. Collected cortical tissue was stored on ice until dissection was complete. The DPBS was then aspirated off. The tissue was resuspended in Earle's balanced salt solution (EBSS, Worthington, USA) containing papain (20 Units papain/mL, 1mM L-cysteine, 0.5mM EDTA; Papain Dissociation System, Worthington, USA) and equilibrated in 10% CO_2 for 1 hour, together with DNase (4000 Units/ml, Worthington, USA), according to the manufacturer's instructions. The tissue was digested for 15 min at 37°C in 5% CO_2 incubator with flick-mixing every 5 min. Digested tissue was triturated approximately 15 times with a fire-polished glass pipette and non-dissociated tissue allowed to settle. The supernatant was then layered onto a step gradient cushion of bovine serum albumin solution (BSA, 4% (w/v), Sigma) in EBSS or Hank's balanced salt solution (HBSS, Life Technologies) in a 15mL tube and cells were centrifuged at 100g for 5 min. The supernatant was aspirated off and the cells resuspended in 1mL of complete Neurobasal medium (Neurobasal serum free medium [-] glutamine (Gibco) with 2% (v/v) B27 Supplement (Gibco); 1% (v/v) Penicillin-streptomycin (10000U/mL stock, Gibco); 0,25% (v/v) L-Glutamine (200mM stock, Gibco); 1% (v/v) Fetal calf bovine serum (FCS), heat inactivated (SAFC Biosciences)). Cell counts were performed using a haemocytometer and dissociated cells were plated at a density of 7.5 x 10^4 cells/mL by adding complete Neurobasal medium. DPBS were added to plate between the wells to help stop them drying out.

At 1 DIV, the mitotic inhibitor fluordeoxyuridine and uridine (FUdR; 1:1000 concentration of 20mM stock of each nucleoside - Sigma) was applied to inhibit glial growth.

4.2.2   Transfection of cultured neurons

At 6 DIV, conditioned medium from neuron cultures to be transfected was collected and retained at 37°C. Coverslips were rinsed quickly with pre-warmed Neurobasal medium then pre-warmed Neurobasal medium (without additives) that had been pre-equilibrated with 5% CO_2 in air, was added to each well. Cells were transfected with different combinations of the following mammalian expression plasmids (Rab5-GFP, Rab11-YFP, TfR-mCherry, SNX17-GFP, SNX27-GFP or Sez-6tII-FLAG) using Lipofectamine 2000 (Life Technologies) according to the manufacturer's instructions. 1μg of DNA was diluted in 25μL Neurobasal and 1.5μL of Lipofectamine 2000 was diluted in 25μL Neurobasal. The DNA and

Lipofectamine solutions were combined. 50μL of combined DNA/Lipofectamine solution was incubated at room temperature (RT) for 5-15 min and then was dropped onto each coverslip in a circular pattern to make up the total volume to 450μL. Plates were incubated for 45 min at 37°C, 5% CO_2. After incubation, DNA/Lipofectamine solution was removed and replaced with the retained conditioned medium.

4.2.3 Immunostaining of cultured-transfected neurons

4.2.3.1 Cell fixation

At 7DIV (12-15 hours after transfection), coverslips were rinsed once in phosphate buffered saline (PBS) for 5 min and then fixed by application of 4% (w/v) paraformaldehyde (PFA) in Phosphate Buffer (PB) for 7 min at RT. PFA/PB was then aspirated off and coverslips were rinsed 3x5 min in PBS. Then coverslips were stored at 4°C in PBS until ready to stain.

4.2.3.2 Immunostaining and mounting

After fixation, the cortical cultures were blocked and permeabilized with 5% (w/v) BSA and 0.1% (v/v) Triton-X-100 in PBS for 1 hour at RT. Then cells were washed 3x5 min with PBS. The relevant primary antibodies (Table 1), diluted to the appropriate concentration in blocking solution, were applied but were also omitted from one well for each condition in order to control for non-specific secondary antibody staining.

After overnight incubation at RT (≈ 20 hours), cells were washed 3x5 min in PBS followed by incubation for 2 hours with the appropriate secondary antibody (Table 2) at RT, protected from light. The secondary antibody was diluted to the appropriate concentration in blocking solution with 5% (w/v) BSA and 0.3% (v/v) Triton-X-100 in PBS.

Cells were rinsed 3 times with PBS and once with MilliQ water before coverslips were mounted on Superfrost Plus slides using mounting medium (DAKO, Denmark) and allowed to dry overnight. Slides were protected from light and stored at 4°C before imaging.

Primary Ab raised against	Species Ab raised in	Dilution	Company	Catalogue number	Target molecules in this study
GFP	Chicken	1:2000	Abcam	ab13970	Rab5 Rab 11 SNX17 SNX27
FLAG	Mouse	1:1000	Sigma	F1804	Sez-6tII
Sez-6	Rabbit	1:1000	Produced in-house		
SNX1	Rabbit	1:2000	Kind gift from Paul Gleeson		
Rab11	Mouse	1:1000	BD Transduction Laboratories	610657	
TfR-mCherry	Mouse	1:1000	Novus	NBP 1-96752	

Table 1 : Primary antibodies used in this study

Secondary Ab raised against	Species Ab raised in	Dilution	Company	Catalogue number	Target molecules in this study
Alexa Fluor 488 conjugated anti-**chicken** IgG (H+L)	Goat	1:1000	Molecular Probes	A-11039	GFP
Alexa Fluor 488 conjugated anti-**mouse** IgG (H+L)	Donkey	1:1000	Life Technologies	A-21202	FLAG Rab 11
Alexa Fluor 594 conjugated anti-**mouse** IgG (H+L)	Donkey	1:1000	Molecular Probes	A-21203	TfR-mCherry
Alexa Fluor 594 conjugated anti-**rabbit** IgG (H+L)	Goat	1:1000	Molecular Probes	A-11037	Sez-6 SNX1

Table 2 : Secondary antibodies used in this study.

4.2.4   Analysis of cultured neurons

4.2.4.1   *Imaging*

Mounted coverslips were imaged using a Carl Zeiss Axio Imager M1 microscope equipped with a Laser Scanning Confocal Microscope (LSM 5) Pascal. If DAPI staining was used, coverslips were imaged using a Carl Zeiss Axio Imager Z1 microscope equipped with a LSM 510 Meta. All cells with a normal appearing morphology (indicating that they were healthy at fixation) were identified and selected at random by eye. 20 neurons per coverslip had been acquired with a 63x oil lens. Eight-bit Z-stack digital images of the fluorescence emission at both 488 and 594 nm were converted into merged maximum intensity projection images using Zen 2009 software (Zeiss, Germany).

4.2.4.2   Image analysis

Neurons were placed on a black background layer and montages were produced using ImageJ software (National Institutes of Health). Initially, a qualitative analysis was done by evaluating the extent of overlap of the different signals (overlay of the green and red images results in yellow if the same structures are labelled). As it is difficult to objectively perform colocalization analyses based on visual inspection, a quantitative correlation was estimated using Imaris software (Bitplane). A volume of the two-dimensional image stacks was created to obtain three-dimensional representations of single neurons. A region of interest (ROI) was selected for the analysis using one of the color channels as a mask. All voxels outside of the ROI defined by the mask channel were ignored for the co-localization analysis. The threshold for each of the signals was fixed individually by contouring (creation of a closed contour line surrounding volumes equal to the intensity of the point selected) within ImarisColoc. A first-pass visual assessment of the image quality (oversaturation, etc.) was performed by generating a scatter plot - for 8-bit images, a 256×256 (zero to 255) scatter plot was generated. In this two-dimensional histogram the intensity of a given pixel in the first channel was used as the x-coordinate of the scatter plot point and the intensity of the corresponding pixel in the second channel as the y-coordinate. The frequency of the red-green voxels combination was represented by voxels color (hot colors representing high values by convention). After reselecting co-localized voxels, colocalization was quantified by computing the Pearson's Correlation Coefficient (PCC).

$$r = \frac{\sum (Ri - \bar{R}) * (Gi - \bar{G})}{\sqrt{\sum (Ri - \bar{R})^2 * \sum (Gi - \bar{G})^2}}$$

Ri and **Gi**: intensity of the red and green channels respectively, of pixel i
R̄ and **Ḡ**: mean intensities of the red and green channels respectively, across the entire image

The PCC, *r*, was used to measure the strength and direction of the linear relationship between the two channels. The *r* value indicates whether the overlap of the voxels in the ROI had a perfect linear correlation (a value of 1), a perfect linear exclusion (a value of -1) or no correlation (a value of 0). The strength of the correlation was categorized according to Evans (1996) whereby an absolute value of *r* between .00 and 0.19 is classified as very weak, between 0.20 and 0.39 as weak, between 0.40 and 0.59 as moderate, between 0.60 and 0.79 as strong and between 0.80 and 1.0 as very strong. The values were presented by *r* ± SEM.

4.3 Determination of whether Sez-6 and SNX17 and/or SNX27 physically interact

4.3.1 Production of purified DNA

In the third part of my study, to investigate whether Sez-6 and SNX17 and/or SNX27 physically interact or form part of an interacting protein complex, high efficiency transformation of plasmids DNAs (encoding SNX17-myc or SNX27-myc) into E. coli was undertaken. To do this, we used the heat shock method (30 secs at 42°C) in accordance with the New England BioLabs (NEB) protocol. Plasmid DNA constructs for SNX17-myc and SNX27-myc were kind gifts from Andrea Bugarcic (Institute for Molecular Bioscience, The University of Queensland). The Myc tag, derived from the human c-myc gene, is a peptide epitope tag used in detection or purification of recombinant proteins. After spreading transformed bacteria onto a selection plate, two colonies per plasmid were picked and used to inoculate Lysogeny broth (LB) medium containing ampicillin. Then plasmids were purified following the PureYield Plasmid Midiprep System (Promega) in order to remove protein, RNA and endotoxin contaminants from purified plasmid DNA. The DNA concentration and purity (absorbance ratios 260/280 and 260/230) were then determined by measuring absorbance using a NanoDrop ND-1000 spectrophotometer.

4.3.2 Transient transfection for recombinant protein production

To produce recombinant proteins, COS-7 cells (African green monkey kidney cells) were grown from frozen stocks in Dulbecco's modified Eagle's medium (DMEM) with 10% FCS, 1% L-glutamine 200mM, 1% Penicillin-streptomycin 10000U/mL; culture reagents from Gibco) until they reached 80% confluence. Cells were transfected with the relevant plasmid constructs (Sez-6-FLAG, SNX17-myc, SNX27-myc, Se6-FLAG and SNX17-myc or Sez-6-FLAG and SNX27-myc) using Lipofectamine 2000 in five different tissue culture dishes (10 cm diameter). A 6th tissue culture dish contained non-transfected COS-cells was used as a control. After protocol optimization, 3μg of DNA was diluted in 500μL DMEM (without additives) and 6μL of Lipofectamine 2000 was diluted in 500μL DMEM (without additives). The DNA and Lipofectamine solutions were combined, incubated at RT for 5-15 min then dropped onto each tissue culture dish and incubated for 6 hours before replacement of the transfection medium with fresh growth medium.

4.3.3   Co-immunoprecipitation

Culture medium was removed before washing cells quickly with PBS. Petri dishes containing transfected COS-7 cells were placed on ice before 1mL of lysis buffer was applied. After optimization, a lysis buffer containing 0.05M Tris pH 7.4, 0.15M NaCl, 2mM EDTA, 1% Triton X-100 (recipe kindly provided by Andrea Bugarcic), phosphatase inhibitors and protease inhibitors (PhosStop and Complete Mini tablets, Roche Applied Science) were used. Cells were detached from the Petri dish by scraping then lysates were incubated at 4°C for 30 min and centrifuged at 14,000 rpm (10 min, 4°C). A sample of the supernatant was kept in order to be processed directly for the western blot. The rest was immunoprecipitated using α-FLAG beads (Sigma Aldrich) and the immunoprecipitated proteins were then processed for the western blot.

4.3.4   Western blot

The separating gel (7.5% acrylamide/bisacrylamide) was poured into a 1.5mm gel chamber and allowed to set. The stacking gel was then poured on top of the polymerized separating gel. A 1.5mm comb was inserted and the gel was allowed to set. The gel chamber was placed into a running tank before the tank was filled with 1x Running Buffer (from 10x Running Buffer: 30g Tris, 148g Glycine, 100mL 10% SDS, up to 1L dH$_2$O).

Both supernatants (lysates and beads) treated with Laemmli buffer (23,5mL distilled water, 2.5 mL Tris pH6.8 1M, 4 mL Glycerol, 8ml 10% SDS, 2ml β-mercaptoethanol, 20µg bromophenol blue) were heated to 95°C for 5 min and put on ice before being loaded (40µL) into the wells in the stacking gel. Protein size standard ladder (7µL, Bio-Rad) was loaded in an adjacent well. Samples were separated by electrophoresis at 100V for 75 min. In a new gel tank filled with 1x transfer buffer (from 10x Transfer Buffer: 30,3g Tris, 144g Glycine, up to 1L dH$_2$O), samples were then transferred to a polyvinylidene fluoride (PVDF) membrane at 100V for 1 hour.

4.3.5 Immunostaining for Western blot membrane protein detection

The membrane was immersed in blocking solution (5% (w/v) skim milk powder in Tris buffered saline with 0.05% Tween 20 (TBST)) and left to gently shake at RT for 30 min. The primary antibody, mouse monoclonal α-myc (Sigma-Aldrich), was diluted at 1:1000 in the blocking solution, added to the membrane which was incubated overnight at 4°C. The membrane was washed (3x15 min) with 1xTBST at RT and then incubated with the secondary antibody (anti-mouse Ig conjugated to horseradish peroxidase (HRP), raised in rabbit, diluted 1:10000 in blocking solution for 1 hour at RT). The membrane was washed again with TBST (3x15 min). Amersham enhanced chemiluminescent substrate solution (ECL) (GE Healthcare Life Sciences, USA) was used to detect reactions with HRP-labeled antibodies. The emission of light signal was then detected on X-ray film.

5 RESULTS

This study was conducted to investigate the hypothesis that Sez-6 is of a great importance in the integration of stimuli that occur at the same time (temporal integration) and at different locations (spatial integration). We also wanted to demonstrate that Sez-6 is trafficked by neuronal SNXs 17 and 27 and could co-operate with them.

To do this, we aimed to determine in a first part the ability of Sez-6 neurons to receive and integrate synaptic information depending on their dendritic morphology. In a second part we wanted to establish the subcellular localizations of Sez-6, SNXs in endosomal compartments and then in a third part, whether Sez-6 and SNXs interact.

## 5.1 Computational simulation of the dendritic integration processes

For investigating the connection between the morphology and the dendritic integration in case of Sez-6 WT and Sez-6 -/- animals, first, we segmented the dendritic arborization of 8 WT (Figure 10, A) and 8 Sez-6 -/- (Figure 10, D) cortical neurons. As previously reported, the Sez-6 -/- neurons had shorter dendrites in average than the WT neurons (Welch t-test, p-value < 0.05, Figure 10, C). We also tested the diameters of these dendrites but did not find significant differences between the neurons (Wilcoxon test, p-value > 0.05, Figure 10, B).
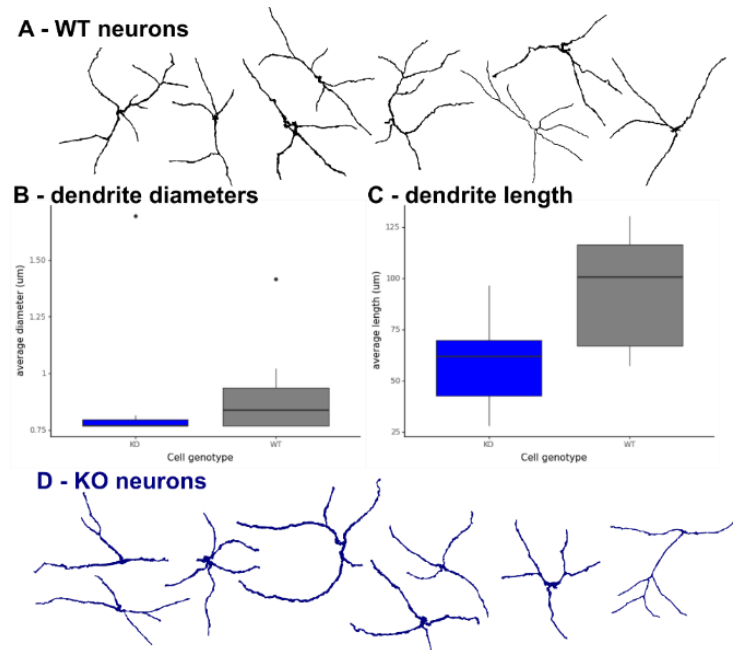
Figure 10 : Morphological differences between the neurons. Sez-6 KO neurons were reported to have shorter neurites, but more branches. We also measured the neurites of the 8-8 neurons (A – WT neurons and D – KO neurons) which were tested during the simulations. The averages of the dendrite diameters were not significantly different (B), but the reported length difference was present in our study (C).

Then according to the compartmentalization modeling, different number of inputs (from 1 to 10) were randomly added on dendritic sections. We observed that the number of inputs is positively correlated to the measured voltages on the soma in all three simulated groups (Pearson's test, $p < 0.01$). However, there are clear tendency that Sez-6 -/- morphology (Sez-6 KO in Figure 11) is a better integrator than WT morphology. If the reported post synaptic density site is included in the model (Sez-6 KO - PSD), the effectiveness of the integration is strongly decreased (Figure 11).
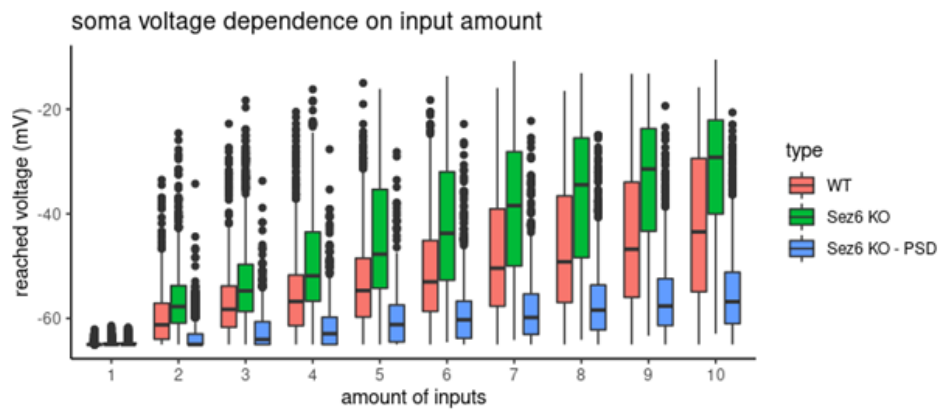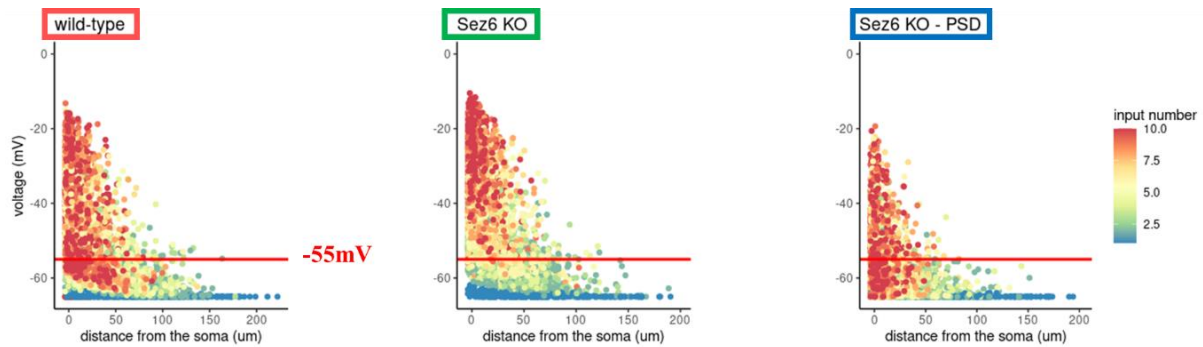

Figure 11 : Voltage of the soma is dependent on the number of inputs (Pearson's test, $p < 0.01$).

We also took in consideration the location of the input on the dendritic sections compared to the soma. We noticed that the input distance is another highly influencing factor of the soma voltage. The closer the input is to the soma, the less the attenuation is visible. Sez-6 KO morphology is better in this aspect, too. Even inputs which are further away from soma generate higher voltages than WT morphology (Pearson's test, $p < 0.01$). The decreased synaptic number (Sez-6 KO - PSD) highly affect the integration processes (Figure 12).
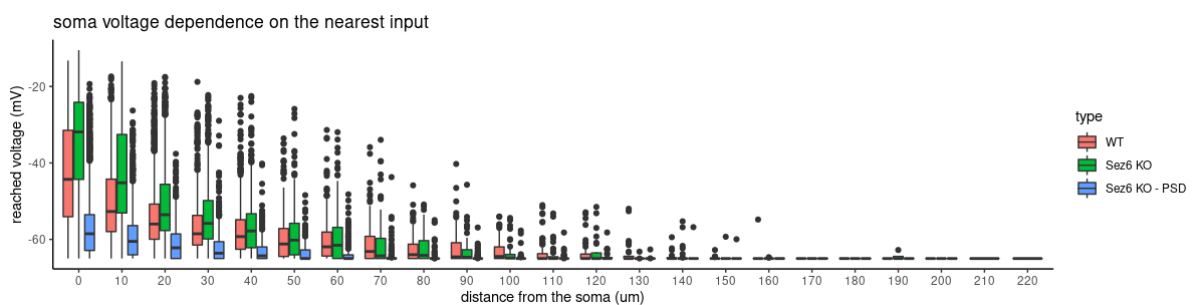

Figure 12 : Voltage of the soma is dependent on the distance of the inputs (Pearson's test, $p < 0.01$).

To resume, the input distance is seen to be to have a strong negative effect in all three-simulation group. On the other side, the input numbers show differences between the different cell's morphology: colors with lower input numbers are mostly located under the threshold (-55 mV) line, while higher input number colors are also present under the threshold in case of WT and Sez-6 KO - PSD cells. In case of Sez-6 KO, the colors representing 6-10 inputs are mostly located above the threshold and reach higher voltages than the other two groups (Figure 13).

Figure 13 : Voltage of the soma is dependent on the neuron type, the input number and the input distance.

Generally, a good integrating cell requires a small number of inputs to activate the cell and for the soma to reach the threshold in order to generate an AP. This is the case of Sez KO morphology, where the AP could be generated in dependence of input number and input distance (Figure 14). WT morphology also has a high probability to reach an AP but still needs a high input number and to be closer to the soma. In case of Sez-6 KO - PSD morphology, the possibility to reach an AP is drastically decreased even in higher input numbers and closer to the soma.
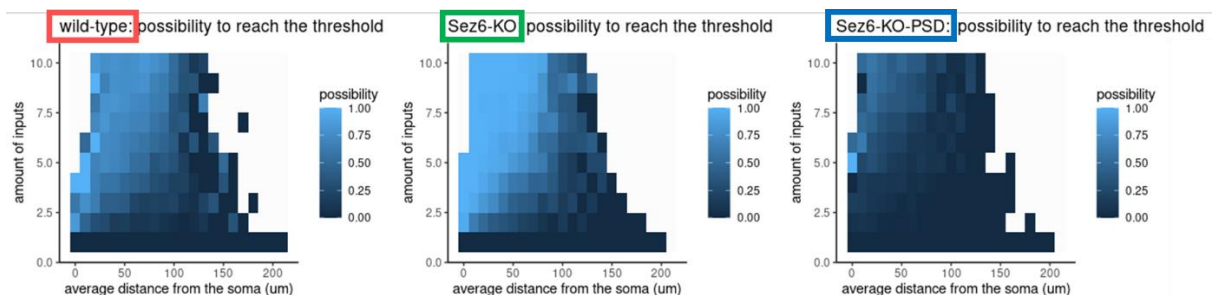
Figure 14 : Possibility of the soma to reach the threshold depending on the neuron type, the input number and the input distance.

The statistical mix-effect model showed that the neuron-type has a clear effect on the maximal voltage that is reached by the soma depending on the input number and the input distance (p- value < 0.001).

5.2   Subcellular localizations of Sez-6, SNX17 and SNX27 in endosomal compartments

As we saw previously, Sez-6 seems to have a great importance in the appropriate dendritic arborization needed to propagate a stimulus in the direction of the soma. However, the expression of Sez-6 and its distribution in neurons are not known as well as its traffic in the different neuronal compartments.

Since SNX are reportedly restricted to particular endosomal compartments, we wished to determine their distribution in neurons. In addition, the respective distributions of the SNXs and Sez-6 were compared in endosomal compartments. Previous data from Gunnersen's laboratory had shown that the SNXs did not exhibit overlap with Rab7 or Rab9, which mark the LE (Soldati et al., 1995). Endosomal compartments were thus only labelled with the EE markers Rab5 (Bucci et al., 1992) or SNX1 (Cozier et al., 2002) or with the RE markers Rab11 (Ullrich et al., 1996) or transferrin receptor (TfR) (Kennedy et al., 2010).

Colocalization analysis was performed involving comparison of the spatial localization of combinations of proteins. These two proteins have either been rendered indirectly fluorescent using transfection or intrinsically fluorescent by immunostaining. To test for non-specific secondary antibody staining, the primary antibodies for each combination were omitted. Results showed no staining with the secondary antibody (data not shown). We conclude that secondary antibodies are specific for their primary antibodies.

5.2.1   Sez-6 exhibits partial overlap with the EE compartment

The first experiments studied whether Sez-6 is localized in EE, marked with fluorescently tagged Rab5 (Rab5-GFP). Cortical neurons were transfected with an expression plasmid for this EE marker and immunostained for Sez-6. Abnormal morphology of neurons was observed after transfection with Rab5-GFP (Figure 15, A). Neurons were looking sick, and the trafficked vesicles were looking big. Reducing the time after transfection from 24 hours to 12-15 hours gave similar results, indicating that overexpression of this marker was detrimental to neuron viability. Another marker, SNX1 was tested as an alternative marker for the EE and was shown to be suitable as Rab5-GFP and SNX1 signals were overlapping (Figure 15, B). Finally, combined immunostaining for Sez-6 and SNX1 was performed to determine whether Sez-6 localizes in the EE (Figure 15, C).
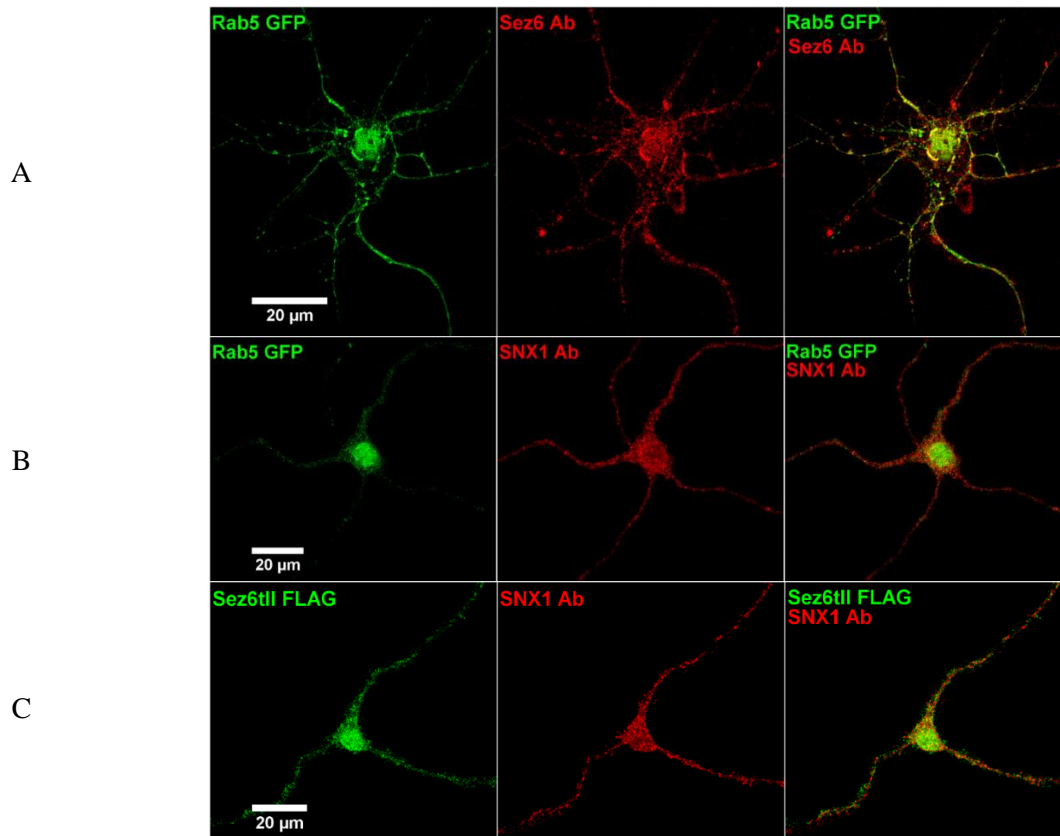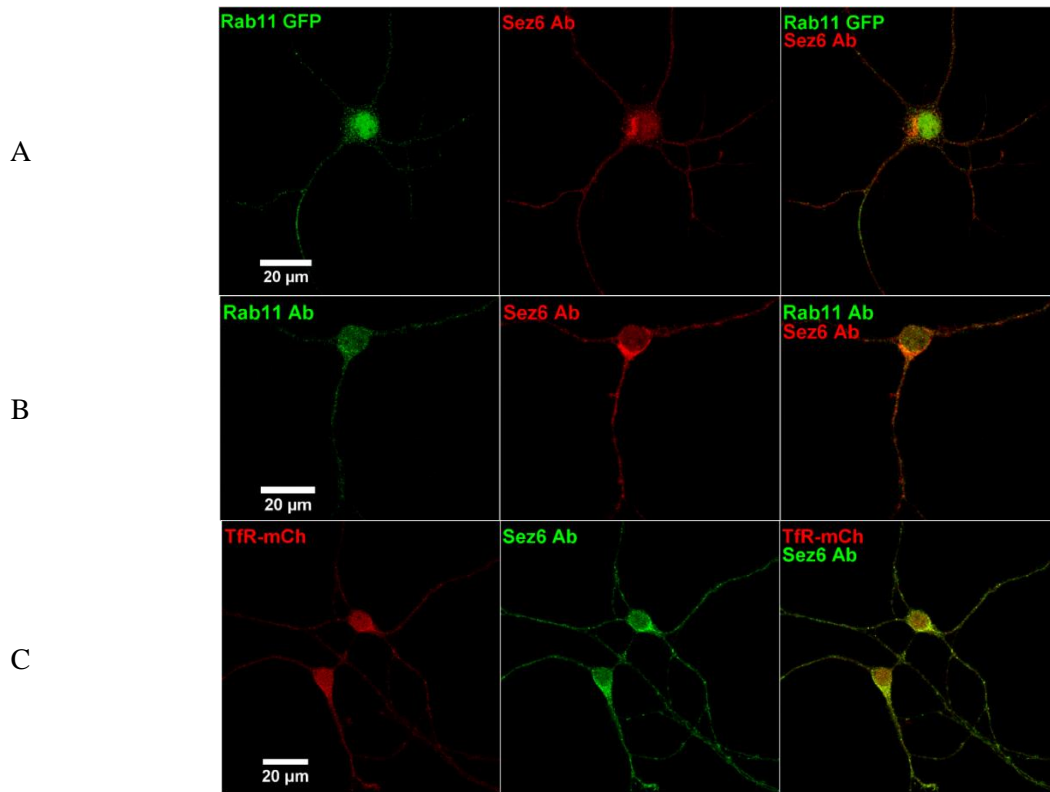
Figure 15 : The subcellular distribution of early endosomal markers (Rab5 and SNX1) and Sez-6 in mouse cortical neurons. Localizations of (A) Rab5 and Sez-6; (B) Rab5 and SNX1; (C) Sez-6 and SNX1.

In scatter plots of the markers shown in B and C, when the green intensity (Rab5 or Sez-6) increased, the red intensity (SNX1) had a tendency to be low (data not shown).

The correlation coefficient r for fluorescence intensities of confocal channels reflects these observations. Indeed, PCC equals to 0.38±0.02 for combination B (Rab5 and SNX1) ranged from 0.30 to 0.49 (N=13). On the other hand, PCC equals to 0.38±0.01 for combination C (Sez-6 and SNX1) ranged from 0.32 to 0.41 (N=11). According to J.D Evans guide (1996), these r values correspond to a weak correlation for both combinations. The PCC was not calculated for the combination A for the reason indicated above: abnormal morphology of neurons was observed after transfection and overexpression of Rab5-GFP.

5.2.2 Sez-6 exhibits moderate overlap with the RE compartment

To study whether Sez-6 is localized in RE, three different methods were used. Either Rab11 transfection (Rab11-GFP; Figure 16, A) or Rab11 immunostaining (Rab11 Ab; Figure 16, B) or TfR transfection (TfR-mCherry, a marker for RE cargo; Figure 16, C), were performed on cortical neurons together with Sez-6.

26

Figure 16 :The subcellular distribution of recycling endosomal markers (Rab11, TfR) and Sez-6 in mouse cortical neurons. Localizations of (A) Rab11-GFP and Sez-6; (B) Rab11 Ab and Sez-6; (C) mCherry-tagged TfR and Sez-6.

For combination C on the scatterplot (Figure 17), when the red intensity (TfR-mCh) increases, the green intensity (Sez-6) also tends to increase. This observation is less obvious for the combinations A and B (Figure 17). Indeed, when the green intensity (Rab11-GFP or Rab11 Ab) increase, the red intensity (Sez-6) has a tendency to be low.
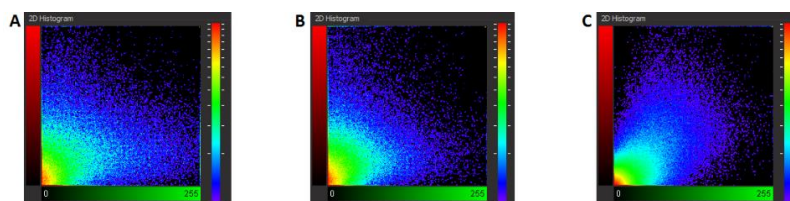

Figure 17 : Scatterplots of red and green pixel intensities from Sez-6 and Rab11-GFP (A); Sez-6 and Rab11 Ab (B); and TfR-mCh and Sez-6 (C).

The correlation coefficient *r* for fluorescence intensities of confocal channels shows a similar situation. Indeed, PCC equals to 0.35±0.02 for combination A (Rab11-GFP and Sez-6) ranged from 0.29 to 0.44 (N=10). Then PCC equals to 0.32±0.02 for combination B (Rab11 Ab and Sez-6) ranged from 0.29 to 0.44 (N=10). And finally, PCC equals to 0.58±0.02 for combination C (TfR and Sez-6) ranged from 0.36 to 0.73 (N=15). According to J.D Evans guide (1996), *r* corresponds to a weak correlation for combination A and B and moderate correlation for combination C.

27

5.2.3   SNX17 and SNX27 weakly localize in EE

Previous data obtained in Gunnersen's laboratory showed that SNX17 and SNX27 were not located in the RE marked by Rab11. Thus, the localization of these SNXs in EE was further studied using SNX1 (Figure 18, A and B), which was a more reliable EE marker than Rab5-GFP (shown in Figure 15, B).
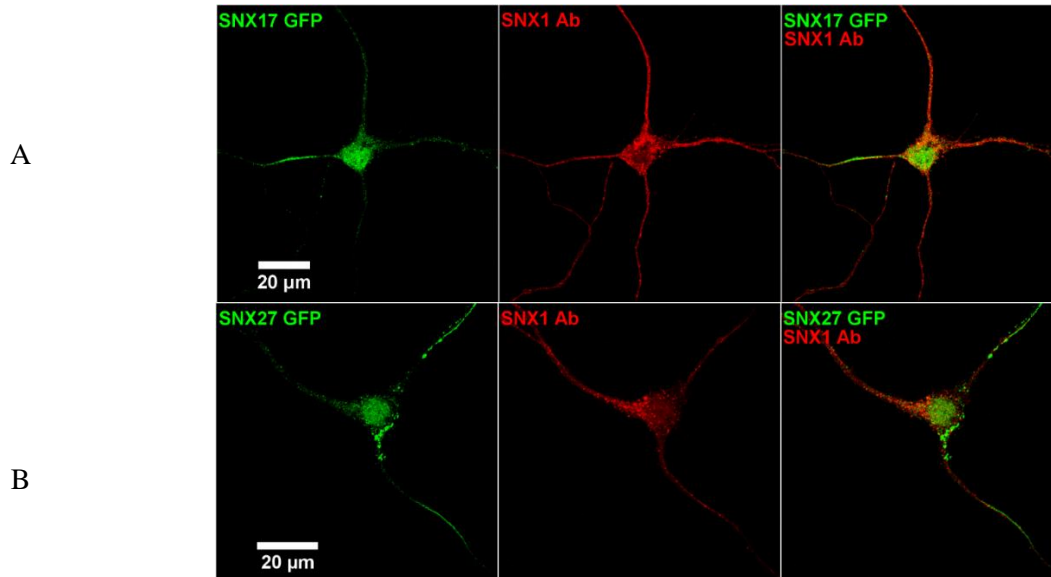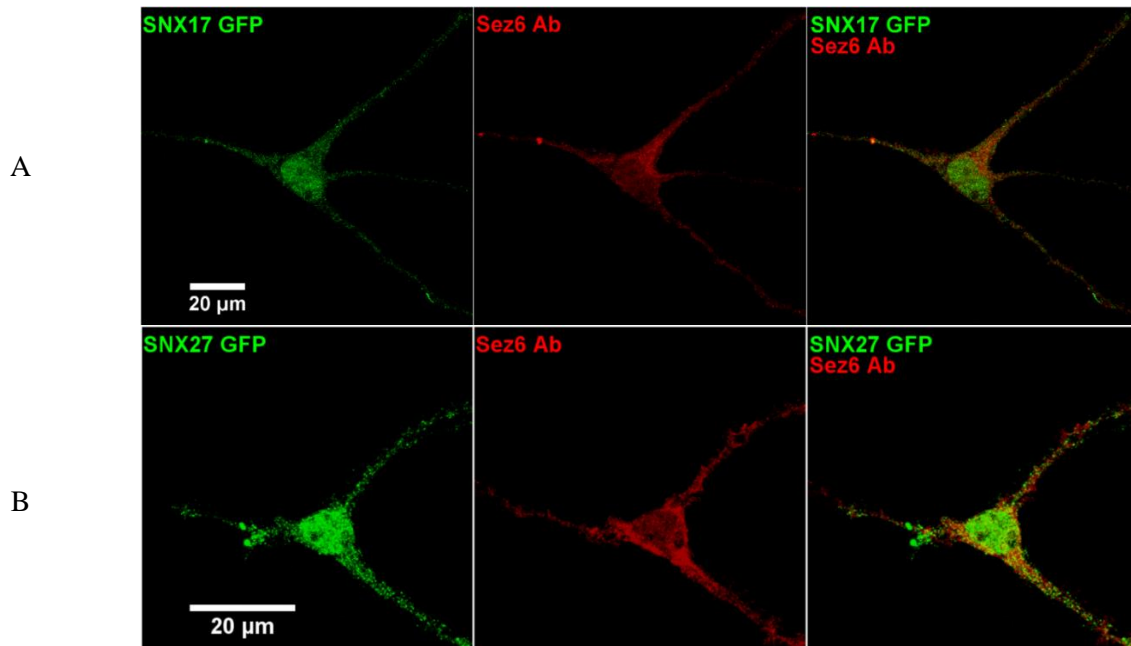

Figure 18 : The subcellular distribution of early endosomal markers (SNX1) and SNXs in mouse cortical neurons. Localization of (A) SNX17 and SNX1; (B) SNX27 and SNX1.

In scatter plots of the markers shown in A and B, when the green intensity (SNX17 or SNX27) increased, the red intensity (SNX1) had a tendency to be low (data not shown).

The correlation coefficient *r* for fluorescence intensities of confocal channels reflects these observations. Indeed, PCC equals to 0.43±0.02 for combination A (SNX17 and SNX1) ranged from 0.32 to 0.52 (N=10). On the other hand, PCC equals to 0.42±0.03 for combination B (SNX27 and SNX1) ranged from 0.25 to 0.53 (N=10). According to J.D Evans guide (1996), *r* corresponds to a weak correlation for both combinations.

5.2.4   Sez-6 weakly co-localizes with SNX17 and SNX27

Previous results indicated that the distribution of Sez-6 and the SNXs overlap in the EE compartments using visual interpretation but are weakly correlated according to the criteria of J.D Evans guide (1996). To investigate this directly, neurons were transfected with fluorescent SNXs and immunostained for Sez-6. As shown in Figure 19, the cellular distribution of both SNX17 and SNX27 overlaps to a large extent with that of Sez-6 (Figure 19, A and B).

Figure 19 : The subcellular distribution of Sez-6 and SNXs in mouse cortical neurons. Localizations of (A) SNX17 and Sez-6; (B) SNX27 and Sez-6.

In scatter plots of the markers shown in A and B, when the green intensity (SNX17 or SNX27) increased, the red intensity (Sez-6) had a tendency to be low (data not shown).

The correlation coefficient r for fluorescence intensities of confocal channels reflects these observations. Indeed, PCC equals to 0.34 ± 0.02 for combination A (SNX17 and Sez-6) ranged from 0.18 to 0.41 (N=10). On the other hand, PCC equals to 0.37 ± 0.02 for combination B (SNX27 and Sez-6) ranged from 0.23 to 0.48 (N=10). According to J.D Evans guide (1996), these values of r correspond to a weak correlation for both combinations.

5.3 Evidence for interaction of Sez-6 and SNX27 from co-immunoprecipitation

The results from the fluorescence imaging experiments (described above) indicated that Sez-6 is weakly localized in the same endosomal compartments as the SNXs in primary neurons. As colocalization merely indicates that two dyes are close in a defined volume and does not directly measure interaction, we examined this issue further by investigating whether these molecules interact when exogenously expressed in a cell line. To do this, co-immunoprecipitation and Western blotting experiments were conducted.

COS-7 cells were co-transfected with FLAG-tagged Sez-6 tII together with either myc-tagged SNX17 (Sez-6+SNX17) or myc-tagged SNX27 (Sez-6+SNX27) (Figure 20). Three controls of these two combinations were done by transfected COS-7 cells with expression constructs for either Sez-6-FLAG (Sez-6) or myc-tagged neuronal SNXs (SNX17 and SNX27) alone. In addition, a non-transfected control without these three controls was performed (No Tfn).
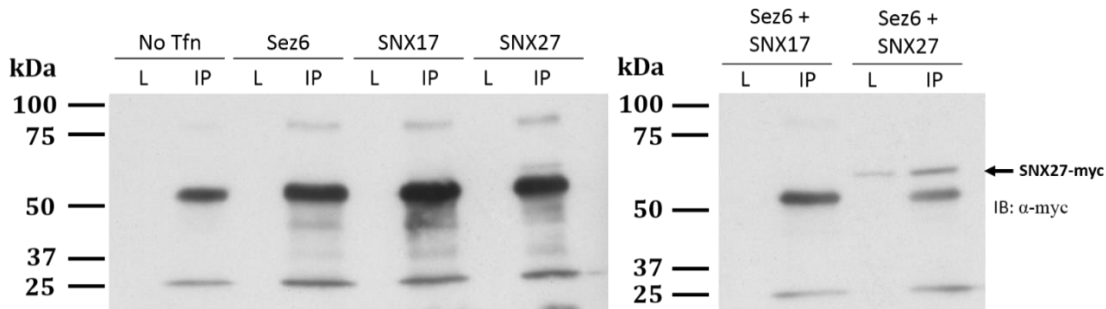
Figure 20 : Co-immunoprecipitation and Western blotting experiments. Lysates (L) and α-FLAG immunoprecipitates (IP) of COS-7 cells transfected with expression constructs for Sez-6tII-FLAG (Sez-6) and myc-tagged neuronal SNXs alone (3 controls: Sez-6, SNX17 and SNX27) or combined (Sez-6 + SNX17 and Sez-6 + SNX27). A control of the 3 controls is the one without transfection (No Tfn). Immunoprecipitated proteins were detected with an α-myc antibody.

Non-specific bands were detected of ~50 kDa and 25 kDa which represent heavy and light chains of mouse anti-FLAG antibody detected by the secondary antibody (rabbit anti-mouse) used for Western blot detection. In addition, the results show that SNX27 (detected using an antibody to the myc-tagged; predicted MW 62 kDa) was co-immunoprecipitated with Sez-6 tII and not abundant when Sez-6 tII was not co-expressed (SNX27+Sez-6 compared to SNX27 alone, Figure 20). On the other hand, SNX17 was not co-immunoprecipitated with Sez-6 tII. Failure to detect exogenously expressed myc-tagged SNX proteins in the lysates (L) before co-immunoprecipitation, as well as the inability to detect immunoprecipitated SNX17 suggested that the expression level of SNXs in this experiment was too low.

6 DISCUSSION

In this study, we first looked at the impact of the expression of the Sez-6 molecule in the processes of dendritic integration in cortical pyramidal cells in mice. To do this, we built computational simulation modelling in order to combine physiological and morphological information into passive cable and compartmental models (Rapp et al., 1994). Once built, we looked at a mixed effects model that allowed us to compare the three types of neurons (WT, Sez-6 KO and Sez-6 KO - PSD), the different input numbers (from 1 to 10) and the location of the input on dendritic sections relative to soma (from 0µm to 220µm).

We observed that more the number of inputs increased, more the voltages measured on the soma increased. Obviously, the increase in the number of stimuli increases the possibility for the soma to reach higher voltage values. In the same way that a large amount of current is needed to evoke dendritic peaks, which means that a large number of synapses must be activated synchronously (Gasparini et al., 2004).

On the other hand, we have noticed that the input distance is another very influential factor of soma voltage. Indeed, the closer the input is to the soma, the less visible the attenuation is. It is also clear that inputs that are closer to soma will have a greater impact on soma voltage as they decrease less easily (Vetter et al., 2001).

By integrating these two data into the morphology, we observed voltage differences between the three groups of neurons, which we predicted. Indeed, the spread of AP in dendrites depends on dendritic morphology (Vetter et al., 2001). At first, we observed that the three groups were impacted by the distance between dendritic stimulation and soma recording. Then from the input point of view, when the input number was between 6 and 10, the voltages reached by the Sez-6 KO neurons were mostly above the threshold of -55mV. On the other hand, with the same amount of stimulation, the voltages reached by WT and Sez-6 KO - PSD neurons rarely exceeded the threshold of -55mV.

In conclusion, we report the surprising result that the morphology of Sez-6 -/- has a clear tendency to be a better integrator than the WT morphology. In general, a good integration cell requires a small number of inputs to activate the cell and for the soma to reach the threshold in order to generate an AP. We can explain this ability by the smaller length of the Sez-6 -/- neurites, which allows to decrease the distance between the site of dendritic stimulation and the recording at the soma level. This trend can also be explained by the

reported increase in the number of dendritic branches per neuron. However, if the reported post-synaptic density decrease is included in the model (Sez-6 KO - PSD), the integration efficiency is greatly reduced. Indeed, the changes in spine density that can occur during development and synaptic plasticity modulate the extent of propagation (Vetter et al., 2001). In this way, as the dendritic integration process is known to have a strong impact on the generation of AP, the coding of neural information is also impacted (Li et al., 2019).

In these experiments we observed that we never managed to reach the threshold to trigger an AP, in the three groups of neurons. In the future, it would therefore be interesting to increase the number of inputs and to be as close as possible to soma in order to observe whether the three groups have the capacity to produce an AP and how many inputs are necessary to trigger it.

If Sez-6 is of great importance in the propagation of a stimulus towards the soma, it is also interesting to know its expression along the dendritic tree and the soma as well as the axon. Thus, secondly, we looked at Sez-6 distribution and its traffic in the different cell compartments of neurons.

To do this, mouse cortical neurons were cultured, transfected, fixed and immunostained to be able to determine the subcellular localization of Sez-6, SNX17 and SNX27. First the overlap between the different signals has been evaluated. Then the spatial colocalization in individual neurons was assessed using scatterplots. And finally, the PCC was calculated to determine whether Sez-6 is enriched in particular subcellular trafficking compartments together with SNXs. Subsequently, recombinant proteins were expressed in COS-cells, co-immunoprecipitated and analyzed by Western blot to determine whether Sez-6 and neuronal SNXs physically interact.

When attempting to mark the EE, we observed that transfection with Rab5-GFP caused neurons to adopt an abnormal morphology, even when the time after transfection was reduced. To avoid this problem, staining of the EE was done using SNX1 antibody. Indeed, SNX1 has previously been shown to exhibit substantial co-localization with EEA1 (Early Endosomal Antigen 1) indicating that it is localized to the EE (Cozier et al., 2002). This approach by using SNX1 is also advantageous because it is more likely to be biologically relevant. Transfection and overexpression of Rab5-GFP may result in aberrant protein distribution whereas SNX1 antibody staining detects the distribution of the native SNX1

protein. As I have concluded that SNX1 staining is a better marker for EE compartment ($r = 0.38\pm0.01$) than the overexpressed fusion protein, I used it for the rest of this study.

Two different methods were used to examine whether Sez-6 is found in the RE. This subcellular compartment was marked with either a GFP-tagged Rab11 (Rab11-GFP) or an expression construct for a TfR-mCh fusion protein. Sez-6 shows moderate colocalization with TfR-mCh in the RE ($r = 0.58\pm0.02$), whereas it was less strongly colocalized with Rab11-GFP ($r = 0.35\pm0.02$). Interestingly, immunostaining with Rab11 antibody revealed a similar correlation with Sez-6 (r = 0.32 ± 0.02). It suggests that the trafficking compartment labeled by TfR is actually more extensive than that labeled by Rab11. TfR, a classic marker for RE trafficking (Kennedy et al., 2010), is ideal because it is constitutively endocytosed and recycled from the endosomal compartment (Roman-Vendrell et al., 2014). Even if the three reporter molecules (TfR-mCh, Rab11-GFP, and Rab11 Ab) distribute to the same intracellular compartments (RE), there is no reason that they should co-occur in fixed proportion to one another. In fact, the ratio of different markers varies considerably within and between structures (Dunn et al., 2011). Thus, these RE markers all mark the RE compartment somewhat differently. These findings are in accordance with a study which has shown that Arf6, Rab11 and TfR define distinct populations of RE (Kobayashi & Fukuda, 2013).

To draw a conclusion about Sez-6 distribution in the EE and/or RE compartments, Sez-6 correlates most closely with the RE-resident TfR and substantially less with the EE-resident, SNX1. Thus Sez-6tII, after being internalized is not retained in the EE but trafficked through this compartment on the way to the RE. These findings are in accordance with the pathway used by TfR which continuously recycles between the plasma membrane and RE through EE, and passes through the Golgi en route to the plasma membrane. However, because only small amounts of TfR were found to be colocalized with EEA1 and GM130 (a Golgi marker), TfR-positive compartments are regarded as RE (Kobayashi & Fukuda, 2013). Thus, TfR could mark closely the trafficking of Sez-6 that we have also surmised is not resident of the EE, but likely to be trafficking though it in this study.

On the other hand, it has previously been reported that SNX17 and SNX27 localize in the EE. Indeed, SNX17 is localized partially in EE (Burden et al., 2004), mainly to the limiting membrane and recycling tubules (van Kerkhof et al., 2005). Furthermore, since SNX27-containing vesicular structures are also marked by EEA1, SNX27 has been shown to be targeted to the EE. Moreover, PtdIns(3)P (to which the PX domain of the SNXs binds) is

primarily enriched in the EE and regulates endosomal recruitment of a large number of PX domain-containing proteins in addition to the SNXs (Cai et al., 2011). In accordance with these results, we found that the subcellular distribution patterns of both SNX17 and SNX27 are positively correlated with the EE markers ($r = 0.43\pm0.02$ and $r = 0.42\pm0.03$, respectively). Concerning the RE, the distribution of GFP-tagged SNXs did not overlap with immunostaining for Rab11 however whether they overlap with TfR has not been tested and this would be an interesting question to address.

This report also established that the cellular distribution of Sez-6 shows some overlap with the distribution patterns of SNX17 ($r = 0.34\pm0.02$) and SNX27 ($r = 0.37\pm0.02$). Even though relatively weak correlations were observed for all the combinations tested, this does not mean that the protein pairs are not colocalized in particular subcellular trafficking compartments. Indeed, we would not expect 100% correlation as the receptor proteins are not resident in these compartments like the Rab proteins, but trafficked through them. If we had a correlation close to 1, this would indicate that Sez-6 and the SNXs were trafficked together absolutely. This would be unlikely in a biological context even if they physically interact. In addition, we acquired 8-bit Z-stack digital images in this study which results in lower PCC values because of compression of the signal range. This problem is minimized when 10- or 12-bit images are used (Adler & Parmryd, 2010). Furthermore, the PCC has been measured for the entire neuron and not for a subregion (e.g. of dendritic arbor, cell body, etc.). In this case, the PCC could under-represent the degree of correlation between the two probes in particular subregions (Dunn et al., 2011). Additional PCC values could thus be measured in ROI that sample only dendrites, cell bodies or axons. Indeed, careful outlining of the region in which two probes may potentially distribute is critical to accurate measurement of the PCC.

The neuron-enriched SNX bind to the NPxY motifs of their cargo molecules via a FERM-like domain and SNX27 has an additional PDZ domain. The co-immunoprecipitation experiments show preliminary evidence that Sez-6 is interacting with SNX27, which is plausible, as the membrane-bound forms of Sez-6 contain both an NPxY motif, as well as a putative PDZ binding domain in their intracellular regions. However, the co-immunoprecipitation didn't show an interaction between Sez-6 and SNX17. These results are consistent with previous unpublished results from Gunnersen's laboratory and provide good evidence for a real interaction between Sez-6 and SNX27. It indicates that binding between Sez-6 and SNX27 is via the PDZ domain of SNX27 which is not present in SNX17. To

investigate this hypothesis, deletion constructs could be used to work out whether the NPxY domain, the putative PDZ interaction domain or both domains of Sez-6 were needed for the interaction and whether the FERM or PDZ domains of SNX27 were important.

Moreover, there is a need to optimize the protocol of co-immunoprecipitation and Western blot in order to enhance expression levels of SNX17 and SNX27. In addition, confirmation of these previous results using a different combination of primary/secondary antibody combination would avoid the problem of cross-reactivity. For example, we could modify the species used for the primary antibody in immunostaining for Western blot membrane protein detection (e.g. a primary antibody against myc raised in goat instead of mouse). Indeed, this primary antibody is an anti-myc raised in mouse that interacts with the secondary antibody, an anti-mouse antibody raised in rabbit. This secondary antibody also reacts with the primary antibody used during co-immunoprecipitation which is an anti-FLAG antibody also raised in mouse. Cross reactivity occurs because the samples are treated with Laemmli buffer and boiled: the anti-FLAG antibody is detached from the beads and is liberated into the buffer.

If further experiments confirm that Sez-6 binds with SNX27, and maybe SNX17, in neurons, the finding could have important implications for the developing nervous system. As the functions of the two SNXs on the trafficking of Sez-6 might be different, the effects of SNXs on the subcellular distribution of Sez-6 should be distinguished. Specific KO of SNX17 or SNX27 with small interfering RNA (siRNAs which inhibit mRNA gene expression), singly or in combination, could provide insight into how the intracellular levels of Sez-6 are modified by these SNXs.

In conclusion, this work has provided convincing evidence for overlapping subcellular distributions and molecular interaction of Sez-6 and the neuronal SNX17 and SNX27. Considering the importance of receptor trafficking in the maturation of synapses, interactions of neuronal SNXs with Sez-6 might play an important role in the development of dendrites and synapses in the nervous system.

7 ABSTRACT

7.1 English

The brain-specific protein, Seizure-related gene-6 (Sez-6), plays an important role in the development of appropriate neuronal circuitry in the mammalian central nervous system. Especially, Sez-6 is an essential regulator of dendritic branching, dendritic spine formation and excitatory synapse numbers.

In this manner Sez-6 -/- animals have been shown to possess morphologically different neurons and dendritic arborization. Indeed, Sez-6 -/- mice exhibit an excess of short dendrites, an excessive neurite branching and a reduced spine density relative to WT neurons. Similarly, a greater proportion of spines were observed on dendrites of control cortical neurons than on Sez-6 -/- neurons.

Based on these morphological data, we have simulated the importance of Sez-6 in signal integration processes of the neurons. We show that dendritic arborization of Sez-6 -/- animals would be a more effective integrator of stimuli that occur at the same time (temporal integration) and at different locations (spatial integration). Indeed, the ability of neurons to receive and integrate synaptic information depends to an extent on their dendritic morphology. However, when the previously announced decreasing number of synapses for Sez 6 -/- was involved in the model, the quality of the signal integration process was drastically reduced.

The signal transduction could also be impacted by endosomal trafficking which is a key mechanism that drives nascent synapse development. The transmembrane cell-surface isoform Sez-6 tII can undergo endocytosis. Transmembrane proteins are continuously shuttled from the endosomal compartment to the neuronal plasma membrane by highly regulated and complex trafficking steps. These events are involved in many homeostatic and physiological processes such as neuronal growth, signaling, learning and memory among others. However, whether the trafficking and cell-surface distribution of Sez-6 is regulated, and how transmembrane Sez-6 is distributed amongst these various compartments, is not known. In the case of Sez-6, the neuronal SNX17 and SNX27 could be involved in regulating its function as they recognize amino acid motifs similar to those in the cytoplasmic tail of Sez-6 tII. We show here that the distribution of Sez-6 and SNXs exhibits partial overlap with the early

endosome and that Sez-6 is partially localized in the recycling endosome. Furthermore, we provide evidence for interaction of Sez-6 and SNX27.

Considering our results, the importance of receptor trafficking in the maturation of synapses, plus the interactions of SNXs with Sez-6 and finally the signal integration processes of the neurons might play an important role in the development of dendrites and synapses as well as the connection circuits in the nervous system.

7.2   Hungarian

A kizárólag az agyban expresszálódó Seizure-related gene-6 (Sez-6) fontos szerepet játszik az idegsejtek kapcsoltságának kialakulásában az emlős központi idegrendszerben. Sez-6 regulálja a dendritek elágazását és aktiváló típusú szinaptikus tüskék formálódását.

Ennek megfelelően a Sez-6 génkiütött (Sez-6 -/-) állatokban eltérő morfológiájú neuronokat és módosult dendritikus arborizációt figyeltek meg. A Sez-6 -/- egerek rövidebb és erősebben elágazó dendritfával rendelkeznek, mint vadtípusú társaik. Ugyanakkor kevesebb szinaptikus tüske figyelhető meg az esetükben.

Ezeken az anatómia megfigyeléseken alapuló szimulációkat végeztünk, hogy megvizsgáljuk, hogyan befolyásolja a Sez-6 géntermék jelenléte illetve hiánya által kialakított morfológia az állatok neuronjainak jelintegrációs képességét. Kimutattuk, hogy a Sez-6 -/- állatok idegsejtjei sokkal hatékonyabban összegzik az egy időben, de a dentritfa különböző helyeire érkező aktiváló jeleket (hatékonyabb a térbeli jelintegrációjuk). Azonban, amennyiben a szimulációban nem csak a morfológiai eltérések szerepeltek, hanem a megfigyelt szinapszis szám csökkenést is figyelembe vettük, drasztikusan csökkent a sejtek jelintegrációs képessége a vadtípusú neuronokéhoz viszonyítva.

A jelátvitelt az idegsejtek endoszómális szállítórendszere is befolyásolhatja, ami szintén jelentős szerepet játszik a szinapszisok érésében és fenntartásában. A sejtfelszínen megtalálható Sez-6 tII-es izoforma endocitózissal visszavehető a felszínről. A neuronok sejtfelszíni fehérjéi folyamatosan vándorolnak a felszín és a citoplazmában lévő endoszómális rendszer között. Mozgásukat azonban erősen szabályozott módon végzik. A vándorlás lépései homeosztatikus és élettani folyamatokat is befolyásolnak, így a neuronális növekedést, jelátvitel, tanulási és memória folyamatokat. Azonban a Sez-6 ezen folyamatokban betöltött szerepét, illetve megoszlását a különböző kompartmentek között, még nem ismerjük. A Sez-6

esetében a neuronális nexinek egy csoportja (neuronal sorting nexins), a SNX17 és a SNX27, lehet felelős az endocitotikus folyamatokért. Ezek a fehérjék hasonló aminosav motívumokat ismernek fel, mint amilyen a Sez-6 tII citoplazmatikus végén elhelyezkedő láncon találhatók. Kimutattuk, hogy a Sez-6 és ezek a nexin fehérjék részleges átfedést mutatnak a korai endoszómális rendszerben, valamint a Sez-6 a recirkulációt lehetővé tevő endoszómális kompartmentben is nagy mennyiségben fordul elő. Továbbá sikerült kimutatni a Sez-6 és a SNX27 interakcióját is.

Eredményeinket figyelembe véve, a Sez-6 kiemelt szerepet játszhat a szinapszisok érési folyamataiban és a szignáltranszdukciós lépésekben, valamint a neuronális kapcsolatok megfelelő kialakításában.

8   References

1. Adler J, Parmryd I (2010) Quantifying colocalization by correlation: the Pearson correlation coefficient is superior to the Mander's overlap coefficient. Cytometry A 77:733–742. doi: 10.1002/cyto.a.20896

2. Ahmari SE, Smith SJ (2002) Knowing a nascent synapse when you see it. Neuron 34:333–336. doi: 10.1016/s0896-6273(02)00685-2

3. Bucci C, Parton RG, Mather IH, Stunnenberg H, Simons K, Hoflack B, Zerial M (1992) The small GTPase rab5 functions as a regulatory factor in the early endocytic pathway. Cell 70:715–728. doi: 10.1016/0092-8674(92)90306-w

4. Burden JJ, Sun X-M, García ABG, Soutar AK (2004) Sorting motifs in the intracellular domain of the low density lipoprotein receptor interact with a novel domain of sorting nexin-17. J Biol Chem 279:16237–16245. doi: 10.1074/jbc.M313689200

5. Cai L, Loo LS, Atlashkin V, Hanson BJ, Hong W (2011) Deficiency of sorting nexin 27 (SNX27) leads to growth retardation and elevated levels of N-methyl-D-aspartate receptor 2C (NR2C). Mol Cell Biol 31:1734–1747. doi: 10.1128/MCB.01044-10

6. Cozier GE, Carlton J, McGregor AH, Gleeson PA, Teasdale RD, Mellor H, Cullen PJ (2002) The phox homology (PX) domain-dependent, 3-phosphoinositide-mediated association of sorting nexin-1 with an early sorting endosomal compartment is required for its ability to regulate epidermal growth factor receptor degradation. J Biol Chem 277:48730–48736. doi: 10.1074/jbc.M206986200

7. Dalby B, Cates S, Harris A, Ohki EC, Tilkins ML, Price PJ, Ciccarone VC (2004) Advanced transfection with Lipofectamine 2000 reagent: primary neurons, siRNA, and high-throughput applications. Methods 33:95–103. doi: 10.1016/j.ymeth.2003.11.023

8. Dunn KW, Kamocka MM, McDonald JH (2011) A practical guide to evaluating colocalization in biological microscopy. Am J Physiol Cell Physiol 300:C723-742. doi: 10.1152/ajpcell.00462.2010

9. Gally, S E, Je R, Jl B (2004) A transmembrane protein required for acetylcholine receptor clustering in Caenorhabditis elegans. Nature 431. doi: 10.1038/nature02893

10. Gasparini, M M, Jc M (2004) On the initiation and propagation of dendritic spikes in CA1 pyramidal neurons. The Journal of neuroscience : the official journal of the Society for Neuroscience 24. doi: 10.1523/JNEUROSCI.2520-04.2004

11. Grant BD, Donaldson JG (2009) Pathways and mechanisms of endocytic recycling. Nat Rev Mol Cell Biol 10:597–608. doi: 10.1038/nrm2755

12. Gunnersen JM, Kim MH, Fuller SJ, De Silva M, Britto JM, Hammond VE, Davies PJ, Petrou S, Faber ESL, Sah P, Tan S-S (2007) Sez-6 proteins affect dendritic arborization patterns and excitability of cortical pyramidal neurons. Neuron 56:621–639. doi: 10.1016/j.neuron.2007.09.018

13. Kennedy MJ, Davison IG, Robinson CG, Ehlers MD (2010) Syntaxin-4 defines a domain for activity-dependent exocytosis in dendritic spines. Cell 141:524–535. doi: 10.1016/j.cell.2010.02.042

14. van Kerkhof P, Lee J, McCormick L, Tetrault E, Lu W, Schoenfish M, Oorschot V, Strous GJ, Klumperman J, Bu G (2005) Sorting nexin 17 facilitates LRP recycling in the early endosome. EMBO J 24:2851–2861. doi: 10.1038/sj.emboj.7600756

15. Kim MH, Gunnersen JM, Tan S-S (2002) Localized expression of the seizure-related gene SEZ-6 in developing and adult forebrains. Mech Dev 118:171–174. doi: 10.1016/s0925-4773(02)00238-1

16. Kim Y, Ha CM, Chang S (2013) SNX26, a GTPase-activating protein for Cdc42, interacts with PSD-95 protein and is involved in activity-dependent dendritic spine formation in mature neurons. J Biol Chem 288:29453–29466. doi: 10.1074/jbc.M113.468801

17. Kobayashi H, Fukuda M (2013) Arf6, Rab11 and transferrin receptor define distinct populations of recycling endosomes. Commun Integr Biol 6:e25036. doi: 10.4161/cib.25036

18. Kuhn P-H, Koroniak K, Hogl S, Colombo A, Zeitschel U, Willem M, Volbracht C, Schepers U, Imhof A, Hoffmeister A, Haass C, Roßner S, Bräse S, Lichtenthaler SF (2012) Secretome protein enrichment identifies physiological BACE1 protease substrates in neurons. EMBO J 31:3157–3168. doi: 10.1038/emboj.2012.173

19. Lee J, Retamal C, Cuitiño L, Caruano-Yzermans A, Shin J-E, van Kerkhof P, Marzolo M-P, Bu G (2008) Adaptor protein sorting nexin 17 regulates amyloid precursor protein trafficking and processing in the early endosomes. J Biol Chem 283:11501–11508. doi: 10.1074/jbc.M800642200

20. Li S, Liu N, Zhang X, McLaughlin DW, Zhou D, Cai D (2019) Dendritic computations captured by an effective point neuron model. Proc Natl Acad Sci U S A 116:15244–15252. doi: 10.1073/pnas.1904463116

21. McAllister AK (2000) Cellular and molecular mechanisms of dendrite growth. Cereb Cortex 10:963–973. doi: 10.1093/cercor/10.10.963

22. Osaki G, Mitsui S, Yuri K (2011) The distribution of the seizure-related gene 6 (Sez-6) protein during postnatal development of the mouse forebrain suggests multiple functions for this protein: an analysis using a new antibody. Brain Res 1386:58–69. doi: 10.1016/j.brainres.2011.02.025

23. Ran Y, Huang Z, Baden T, Schubert T, Baayen H, Berens P, Franke K, Euler T (2020) Type-specific dendritic integration in mouse retinal ganglion cells. Nat Commun 11:2101. doi: 10.1038/s41467-020-15867-9

24. Rapp M, Segev I, Yarom Y (1994) Physiology, morphology and detailed passive models of guinea-pig cerebellar Purkinje cells. J Physiol 474:101–118. doi: 10.1113/jphysiol.1994.sp020006

25. Rink J, Ghigo E, Kalaidzidis Y, Zerial M (2005) Rab conversion as a mechanism of progression from early to late endosomes. Cell 122:735–749. doi: 10.1016/j.cell.2005.06.043

26. Roman-Vendrell C, Chevalier M, Acevedo-Canabal AM, Delgado-Peraza F, Flores-Otero J, Yudowski GA (2014) Imaging of kiss-and-run exocytosis of surface receptors in neuronal cultures. Front Cell Neurosci 8:363. doi: 10.3389/fncel.2014.00363

27. Shimizu-Nishikawa K, Kajiwara K, Kimura M, Katsuki M, Sugaya E (1995) Cloning and expression of SEZ-6, a brain-specific and seizure-related cDNA. Brain Res Mol Brain Res 28:201–210. doi: 10.1016/0169-328x(94)00203-q

28. Shimizu-Nishikawa K, Kajiwara K, Sugaya E (1995) Cloning and characterization of seizure-related gene, SEZ-6. Biochem Biophys Res Commun 216:382–389. doi: 10.1006/bbrc.1995.2635

29. Soldati T, Rancaño C, Geissler H, Pfeffer SR (1995) Rab7 and Rab9 are recruited onto late endosomes by biochemically distinguishable processes. J Biol Chem 270:25541–25548. doi: 10.1074/jbc.270.43.25541

30. Sönnichsen B, De Renzis S, Nielsen E, Rietdorf J, Zerial M (2000) Distinct membrane domains on endosomes in the recycling pathway visualized by multicolor imaging of Rab4, Rab5, and Rab11. J Cell Biol 149:901–914. doi: 10.1083/jcb.149.4.901

31. Teasdale RD, Collins BM (2012) Insights into the PX (phox-homology) domain and SNX (sorting nexin) protein families: structures, functions and roles in disease. Biochem J 441:39–59. doi: 10.1042/BJ20111226

32. Ullrich O, Reinsch S, Urbé S, Zerial M, Parton RG (1996) Rab11 regulates recycling through the pericentriolar recycling endosome. J Cell Biol 135:913–924. doi: 10.1083/jcb.135.4.913

33. Vetter P, Roth A, Häusser M (2001) Propagation of action potentials in dendrites depends on dendritic morphology. J Neurophysiol 85:926–937. doi: 10.1152/jn.2001.85.2.926

9   <u>Acknowledgements</u>

NYILATKOZAT

Alulírott …*Floriane LOUBOUTIN*… nyilatkozom, hogy diplomamunkám, melynek címe *Neuronal sorting nexins and Seizure-related gene 6 trafficking and their influence in the dendritic integration* …………………………………………………. tartalmi és formai szempontból teljes mértékben megegyezik azonos című, a …*2022*… évi TDK konferencián szerepelt dolgozatommal.

Budapest, *7th November 2022*

…………………………………………..

a hallgató neve és aláírása

HuVetA
ELECTRONIC LICENSE AGREEMENT AND COPYRIGHT DECLARATION*

Name: Floriane LOUBOUTIN

Contact information (e-mail): floriane.louboutin@yahoo.fr

Title of document (to be uploaded): Neuronal sorting nexins and Seizure-related gene 6 trafficking and their influence in the dendritic integration

Publication data of document: 2022

Number of files submitted: 1

By accepting the present agreement the author or copyright owner grants non-exclusive license to HuVetA over the above mentioned document (including its abstract) to be converted to copy protected PDF format without changing its content, in order to archive, reproduce, and make accessible under the conditions specified below.

The author agrees that HuVetA may store more than one copy (accessible only to HuVetA administrators) of the licensed document exclusively for purposes of secure storage and backup, if necessary.

You state that the submission is your original work, and that you have the right to grant the rights contained in this license. You also state that your submission does not, to the best of your knowledge, infringe upon anyone's copyright. If the document has parts which you are not the copyright owner of, you have to indicate that you have obtained unrestricted permission from the copyright owner to grant the rights required by this Agreement, and that any such third-party owned material is clearly identified and acknowledged within the text of the licensed document.

The copyright owner defines the scope of access to the document stored in HuVetA as follows (**mark the appropriate box with an X)**:

[X] I grant unlimited online access,

[ ] I grant access only through the intranet (IP range) of the University of Veterinary Medicine,

[ ] I grant access only on one dedicated computer at the Ferenc Hutÿra Library,

[ ] I grant unlimited online access only to the bibliographic data and abstract of the document.

Please, define the **in-house accessibility of the document** by marking the below box with an **X** :

I grant in-house access (namely, reading the hard copy version of the document) at the Library.

If the preparation of the document to be uploaded was supported or sponsored by a firm or an organization, you also declare that you are entitled to sign the present Agreement concerning the document.

The operators of HuVetA do not assume any legal liability or responsibility towards the author/copyright holder/organizations in case somebody uses the material legally uploaded to HuVetA in a way that is unlawful.

Date: Budapest, ...24..day ...10.....month...2022....year

_____
Author/copyright owner
signature

_____

Thesis progress report for veterinary students

Name of student: Louboutin Floriane Marie Elisabeth

Neptun code of the student: IFR94N

Name and title of the supervisor: Eszter Berekméri, research fellow

Department: Department of Ecology

Thesis title: Neuronal sorting nexins and Seizure-related gene 6 trafficking and their influence in the dendritic integration

Consultation – 1st semester

	Timing			Topic / Remarks of the supervisor	Signature of the supervisor
	year	month	day		
1.	2022	March	17	TDK project definition	
2.	2022	March	24	NEURON, Python and Anaconda installation	
3.	2022	March	31	Swc files and how to create them	
4.	2022	April	4	Image J installation	
5.	2022	April	13	Swc files import to NEURON	
6.	2022	April	21	Colab, 1st test of the cells	
7.	2022	May	4	Number of inputs to activate an AP	
8.	2022	June	3	Jupyter - Template	

Grade achieved at the end of the first semester: 5 (jeles)

Consultation – 2nd semester

	Timing			Topic / Remarks of the supervisor	Signature of the supervisor
	year	month	day		
1.	2022	July	14	Tracing neurons in Image J	
2.	2022	July	22	Template for working	
3.	2022	July	29	Code running and result visualisation	
4.	2022	Aug	5	Unfit and Fit volume in Image J	
5.	2022	Aug	16	Cable theory, Cable equation	
6.	2022	Sept	6	Modify the KO animal testing protocol	
7.	2022	Sept	27	TDK abstract and thesis	
8.	2022	Nov	13	TDK presentation	

Grade achieved at the end of the second semester: 5 (jeles)

The thesis meets the requirements of the Study and Examination Rules of the University and the Guide to Thesis Writing.

I accept the thesis and found suitable to defence,

....
signature of the supervisor

Signature of the student: ....

Signature of the secretary of the department: ....

Date of handing the thesis in........... ....